ciations of hypervalent radicals produced by neutralization of stable ions.[7] Although we have no rigorous explanation of this phenomenon, it appears that **1** is initially formed in a variety of excited electronic states due to the very fast electron transfer and the virtually random orientation of the ion and neutral counterparts. An unbound electronic state of the neutral will dissociate rapidly on the particular potential energy surface that may be different from that calculated for **1** that leads to the S-O bond rupture. In this model, the branching ratio will depend on the initial electronic state population rather than the dissociation kinetics.

Conclusions

Dimethylhydroxysulfuranyl radical **1** does not survive 4.5 μs after having been formed by vertical neutralization of the dimethylhydroxysulfonium ion, and dissociates exothermically by cleavages of the C-S, O-S, and O-H bonds. No stable equilibrium structure is found for **1** by ab initio calculations that also predict exothermic dissociation. **1** thus represents a transition state rather than an intermediate in the atmospherically important oxidation of dimethyl sulfide with hydroxyl radicals.

Acknowledgment. We gratefully acknowledge the generous financial support by the National Science Foundation (Grant CHEM-9102442), the University of Washington Graduate School Fund, the donors of the Petroleum Research Fund, administered by the American Chemical Society, for partial supports of this work, and the computational support by the Cornell National Supercomputer Facility which receives major funding from the National Science Foundation and the IBM corporation, with additional support from the New York State and the Corporate Research Institute.

Supplementary Material Available: Listing of 6-31G* and 3-21G calculated harmonic vibrational frequencies of sulfur-containing species (1 page). Ordering information is given on any current masthead page.

Formation of $LaCoO_3$ Highly Dispersed on ZrO_2

Noritaka Mizuno,*,† Hiroaki Fujii,‡ Hiroshi Igarashi, and Makoto Misono*

Contribution from the Department of Synthetic Chemistry, Faculty of Engineering, The University of Tokyo, Hongo, Bunkyo-ku, Tokyo 113, Japan. *Received February 5, 1992*

Abstract: The well-characterized La-Co oxide overlayer was prepared on the surface of ZrO_2 powder by impregnating ZrO_2 with aqueous solutions of the mixtures of La and Co acetates followed by calcination at various temperatures. The preparation processes and the structure of La-Co oxide overlayers were investigated in detail by IR, XRD, XPS, EDX, TEM, and adsorption of NO and pyridine. It was concluded that a highly dispersed La-Co oxide overlayer which may have the $LaCoO_3$ perovskite structure was formed. The resulting La-Co/ZrO_2 catalysts showed very high catalytic activities for complete oxidation of propane.

Introduction

Metal oxide overlayers on the surface of metal oxides or metals have attracted much attention in the fields of materials science, electrochemistry, corrosion, heterogeneous catalysis, and so on, owing to their specific surface reactivity and electrical or tribological properties. So, the investigation of the process of growth of the oxide overlayer is interesting for the better understanding and precise control of the surface reactivity and electrical or tribological properties.

Perovskite-type mixed oxides, ABO_3 (A = La, Ca, Sr, Ba, etc.; B = Co, Ti, Mn, etc.), have important physical properties such as ferro-, piezo-, and pyroelectricity, magnetism, electrooptic effects, and superconductivity. In addition, perovskites are good catalysts for various reactions: oxidation of CO and hydrocarbons, reduction of NO and SO_2, hydrogenation and hydrogenolysis of hydrocarbons, etc.[1-3] Perovskites containing Co or Mn show high catalytic activity for the complete oxidation of CO, CH_4, and C_3H_8;[4-10] e.g., the catalytic activity of $La_{0.8}Sr_{0.2}CoO_3$ is comparative to or higher than that of Pt catalysts and $La_{0.9}Ce_{0.1}CoO_3$ was actually used as a commercial catalyst.[11]

Although the perovskite catalysts are thermally more stable and less expensive than noble metal catalysts, the surface area is low. If the perovskites were directly supported on high surface area supports, they would be much more attractive catalysts in practice. However, the solid-state reactions between perovskite components and the support oxides to form other stable mixed oxides often take place. For example, Co-containing perovskites cannot be directly supported on alumina-based oxides, since cobalt atoms are incorporated into the bulk of the support to form a spinel ($CoAl_2O_4$),[6,7] so that the majority of cobalt atoms cannot contribute to the catalytic activity.

In earlier works, perovskite particles were supported on cordierite and alumina by using aqueous slurries containing powdered perovskite, cordierite or alumina, and stearic acid.[8,9] But the reaction between the perovskite particle and support to form less reactive mixed oxides was not avoidable. Recently, several new methods have been attempted,[10,12-18] such as precoating of the

* Author to whom correspondence should be addressed.
† Present address: Catalysis Research Center, Hokkaido University, Sapporo 060, Japan.
‡ Present address: Kuraray Co., Ltd., Kaigan-dori, Okayama 702, Japan.

(1) Voorhoeve, R. J. H. In *Advanced Materials in Catalysis*; Burton, J. J., Garten, R. L., Eds.; Academic Press: New York, 1977; pp 129-180.
(2) Tejuca, L. G.; Fierro, J. L. G.; Tascon, J. M. D. in *Advances in Catalysis*; Eley, D. E., Pines, H., Weisz, P. B., Eds.; Academic Press: San Diego, 1989; Vol. 36, p 237. Misono, M., Lombardo, E. A., Eds. Perovskite. *Catal. Today* **1990**, *8*, 133-275.
(3) Mizuno, N. *Catal. Today* **1990**, *8*, 221-230.
(4) Nakamura, T.; Misono, M.; Uchijima, T.; Yoneda, Y. *Nippon Kagaka Kaishi* **1980**, 1679-1684.
(5) Nakamura, T.; Misono, M.; Yoneda, Y. *J. Catal.* **1983**, *83*, 151-159.
(6) Arnoldy, P.; Moulijn, J. A. *J. Catal.* **1985**, *93*, 38-54.
(7) Massoth, F. E. In *Advances in Catalysis*; Eley, D. E., Pines, H., Weisz, P. B., Eds.; Academic Press: New York, 1978; Vol. 27, pp 265-310.
(8) Gallagher, P. K.; Johnson, D. W., Jr.; Schrey, F. *Mat. Res. Bull.* **1974**, *9*, 1345-1352.
(9) Chien, M. W.; Pearson, I. M.; Nobe, K. *Ind. Eng. Chem. Prod. Res. Dev.* **1975**, *14*, 131-134.
(10) Nudel, J. N.; Umansky, B. S.; Lombardo, E. A. *Appl. Catal.* **1987**, *31*, 275-289.
(11) Tabata, K.; Misono, M. *Catal. Today* **1990**, *8*, 249-261.
(12) Fujii, H.; Mizuno, N.; Misono, M. *Chem. Lett.* **1987**, 2147-2150.

0002-7863/92/1514-7151$03.00/0

supports with less reactive oxides to avoid the reaction of perovskite components with supports,[10,13,14] freeze drying to reduce the macroscopic inhomogeneities,[15,16] and the usage of citrate precursors to obtain high dispersion.[17]

Considerable efforts have also been directed toward the characterization of these materials by using XPS, XRD, TEM, EXAFS, NO–NH_3 reaction, O_2 chemisorption, and so on.[10,14,19-21] However, much remained unelucidated and fundamental studies are necessary particularly in the case of high-temperature processes that are needed, for example, for the preparation of catalysts for combustion such as perovskite-type mixed oxides.

In the previous preliminary communications, we reported that zirconium dioxide (ZrO_2) is very suitable for supporting La–Co and La–Sr–Co oxides.[12,22] It is also known that perovskites are good electrode materials when ZrO_2 is used as solid electrolyte.[23] In the present paper, we have attempted to clarify the preparation processes and the structure of La–Co oxide overlayers in detail by IR, XRD, XPS, EDX, TEM, and adsorption of NO and pyridine, and it was concluded that a highly dispersed La–Co oxide overlayer which very likely had the $LaCoO_3$ perovskite structure was formed. The resulting La–Co/ZrO_2 catalysts showed very high catalytic activities for complete oxidation of propane.

Experimental Section

Catalyst Preparation. ZrO_2 was prepared by the hydrolysis of the zirconium chloride oxide. The hydrolyzed product was calcined at 1123 K for 5 h in air before use as a support. Two ZrO_2 samples having different specific surface areas (15 and 26 $m^2 \cdot g^{-1}$) were prepared. The sample with 15 $m^2 \cdot g^{-1}$ was used unless otherwise stated. It was confirmed by the X-ray diffraction patterns that all ZrO_2 substances have the monoclinic structure. The ZrO_2 samples were impregnated with an aqueous solution of a stoichiometric mixture of lanthanum and cobalt acetates (atomic ratio of Co/La = 1) or with that of lanthanum acetate ($La(OAc)_3$) or cobalt acetate ($Co(OAc)_2$) by the incipient wetness method. The aqueous solution concentrations of $La(OAc)_3$ and $Co(OAc)_2$ were about 7×10^{-2} mol·dm^{-3}. For high levels of loading, the impregnation–drying cycle was repeated several times unless otherwise stated. After final drying at about 373 K, the samples were calcined at 1123 K for 5 h in air unless otherwise stated. Hereafter, the resulting catalysts are denoted by La–Co/ZrO_2. Rhombohedral $LaCoO_3$ was prepared as in the previous paper.[4] Cubic Co_3O_4 or hexagonal La_2O_3 and cubic $La_2Zr_2O_7$ were obtained by the calcination of metal acetates at 1123 and 1273 K, respectively, for 5 h.

Powder X-ray diffraction patterns were recorded on a powder X-ray diffractometer (Rigaku Denki, Rotaflex, RU-200) by using Cu Kα radiation. Specific surface areas were measured by the BET method using N_2 adsorption at 77 K after the pretreatment of the samples in a He stream at 573 K.

Adsorption of NO and Pyridine. NO chemisorption under an equilibrium pressure of about 50 mmHg was measured by the pressure decrease at room temperature with a high-vacuum static system after an evacuation at 773 K for 2 h. IR spectra of pyridine adsorbed were measured as follows. After a self-supporting disk of the sample (40–60 mg, 2 cm in diameter) was treated in an in situ IR cell in circulating O_2 (70 mmHg) at 673 K for 1 h and subsequently evacuated at 673 K for 1 h, it was exposed to pyridine vapor (5–10 mmHg) at room temperature and then evacuated at 403 K. Next the IR spectra were recorded at 298 K with a JIR-10 FT-IR spectrometer (JEOL). The amounts of pyridine adsorbed were evaluated by the integrated intensities of the IR band at 1446 cm^{-1}.

XPS Measurements. Self-supporting disks (about 10 mg, 1 cm in diameter) were used, and the spectra were recorded with a JEOL JPS-90SX spectrometer with a MgKα source (1253.6 eV). The pressure in the chamber was kept at 10^{-8} to 10^{-9} mmHg. The binding energies were corrected by using the values of 285.0 eV for the C 1s peak of the adventituous carbon as an internal standard as described previously.[24] XPS intensity ratios were determined by using the integrated areas of the Co $2p_{3/2}$ and La $3d_{5/2}$ photoelectron lines, and the sum of the integrated areas of Zr $3d_{5/2}$ and Zr $3d_{3/2}$ photoelectron lines, considering the overlapping of the two lines. The surface atomic ratios of Co/La of the samples were calculated from eq 1.[25] For the elements Co and La, the relationship

$$\frac{I_{Co_{2p3/2}}}{I_{La_{3d5/2}}} = \frac{\sigma_{Co}\lambda_{Co}d_{Co}}{\sigma_{La}\lambda_{La}d_{La}} \quad (1)$$

where $I_{Co_{2p3/2}}$ and $I_{La_{3d5/2}}$ are the integrated peak intensities of Co $2p_{3/2}$ and La $3d_{5/2}$ including the satellite line, respectively, σ_{Co} and σ_{La} are the Scofield photoelectron cross sections for Co $2p_{3/2}$ and La $3d_{5/2}$,[26] respectively, λ_{Co} and λ_{La} are the inelastic mean free paths of Co $2p_{3/2}$ and La $3d_{5/2}$, respectively, and d_{Co} and d_{La} are the numbers of Co and La atoms in unit volumes, respectively, was used. λ_{Co} and λ_{La} were assumed to be the same as those from Co $2p_{3/2}$ and La $3d_{5/2}$ in a $LaCoO_3$ perovskite overlayer, respectively (see Discussion). Approximately the same Co/La ratio was obtained when the peak intensities of La $3d_{3/2}$ and Co $2p_{1/2}$ lines were used instead of La $3d_{5/2}$ and Co $2p_{3/2}$, respectively.

Energy Dispersive X-ray Measurements. A transmission electron microscope (JEOL, JEM-2000FX) was used for imaging and energy dispersive X-ray spectroscopy (EDX) to measure the chemical composition of each particle (400–800-Å diameter) of ZrO_2 and La–Co/ZrO_2. The measurements were carried out on ca. 800 particles for respective samples. The observed major families of lines are due to Zr, La, and Co. The quantitative evaluation of the chemical composition was made by using the Cliff–Lorimer factor according to the report by Wang et al.[27]

Reaction. The catalytic oxidation of propane was carried out at 500–673 K with a flow system, after the catalysts (about 0.1 g) were pretreated at 723 K in an O_2 stream, as in previous works.[12,14] Complete oxidation was the only reaction observed. The feed gas was a gas mixture of propane (0.83%), O_2 (33.3%), and N_2 (balance). The steady-state conversion was kept at less than 20% and the linear correlation was confirmed between the conversion (≤20%) and W(weight of catalyst)/F(flow rate). The rates were calculated from the slopes.

Other Measurements. The adsorption experiments in aqueous solutions were carried out as follows. After ZrO_2 (1 g) was stirred for 2 h in an aqueous solution (5 cm^3) of a mixture of $La(OAc)_3$ and $Co(OAc)_2$ (7.3×10^{-2} mol·dm^{-3}), the solution was filtered. The amounts of La and Co ions adsorbed on ZrO_2 were evaluated by the amounts of La and Co ions contained in the filtrate measured by ICP (Nippon Jarrell-Ash Co. Ltd.).

Transmission electron micrographs were obtained with a JEOL JEM 1250 electron microscope (1000 keV; final magnification × 150000). The fitting of planes between La–Co oxide and ZrO_2 in La–Co/ZrO_2 particles was not identified by the electron microscopy of lattice planes because of the small magnification.

Results

Formation of $LaCoO_3$ on ZrO_2. XRD patterns of La–Co/ZrO_2 calcined at 1123 K are shown in Figure 1. Hereafter, the amount of the substance loaded is calculated and expressed by assuming the composition of $LaCoO_3$. No phases other than monoclinic ZrO_2 were observed, and the line intensity of ZrO_2 decreased linearly until the amount of La–Co oxide loaded reached 5.1 wt %. At and above the loading level of 7.5 wt %, the additional lines attributed to the main diffraction lines of $LaCoO_3$ (2θ = 32.9 and 33.3°), $La_2Zr_2O_7$ (28.7°), and Co_3O_4 (36.8°) were observed.

(13) Nudel, J. N.; Umansky, B. S.; Lombardo, E. A. *Appl. Catal.* **1986**, *26*, 339–351.
(14) Mizuno, N.; Fujii, H.; Misono, M. *Chem. Lett.* **1986**, 1333–1336. The effect of supports including ZrO_2 on the formation of $La_{0.8}Sr_{0.2}CoO_3$ perovskite-type mixed oxide will be published in an appropriate journal.
(15) Johnson, D. W., Jr.; Gallagher, P. K.; Schrey, F.; Rhodes, W. W. *Am. Ceram. Soc. Bull.* **1976**, *55*, 520–527.
(16) Johnson, D. W., Jr.; Gallagher, P. K.; Schnettler, F. J.; Vogel, E. M. *Am. Ceram. Soc. Bull.* **1977**, *56*, 785–792.
(17) Zhang, H. M.; Teraoka, Y.; Yamazoe, N. *Appl. Catal.* **1988**, *41*, 137–146.
(18) Teraoka, Y.; Zhang, H. M.; Yamazoe, N. In *Proceedings—9th International Congress on Catalysis, 1988*; Phillips, M. J., Ternan, M., Eds.; The Chemical Institute of Canada: Ottawa, 1988; pp 1984–1991.
(19) Saheh, R. Y.; Wachs, I. E.; Chan, S. S.; Chersich, C. C. *J. Catal.* **1986**, *98*, 102–114.
(20) Ono, T.; Anpo, M.; Kubokawa, Y. *J. Phys. Chem.* **1986**, *90*, 4780–4784.
(21) Nag, N. N. *J. Phys. Chem.* **1987**, *91*, 2324–2327.
(22) Fujii, H.; Mizuno, N.; Misono, M. In *Proceedings—MRS International Meeting On Advanced Materials*; Doyama, M., Somiya, S., Chang, R. P. H., Eds.; Materials Research Society: Pittsburgh, 1989; pp 255–260.
(23) Yamamoto, O.; Takeda, Y.; Kanno, R.; Noda, M. *Solid State Ionics* **1987**, *22*, 241–246.
(24) Mizuno, N.; Yamato, M.; Tanaka, M.; Misono, M. *Chem. Mater.* **1989**, *1*, 232–236.
(25) Carter, W. J.; Schweitzer, G. K.; Carlson, T. A. *J. Electron Spectrosc. Relat. Phenom.* **1974**, *5*, 827–835.
(26) Scofield, J. H. *J. Electron Spectrosc. Relat. Phenom.* **1976**, *8*, 129–137.
(27) Wang, Z. L.; Colliex, C.; P.-Boncour, V.; P.-Guegan, A.; Achard, J. C.; Barrault, J. *J. Catal.* **1987**, *105*, 120–143.

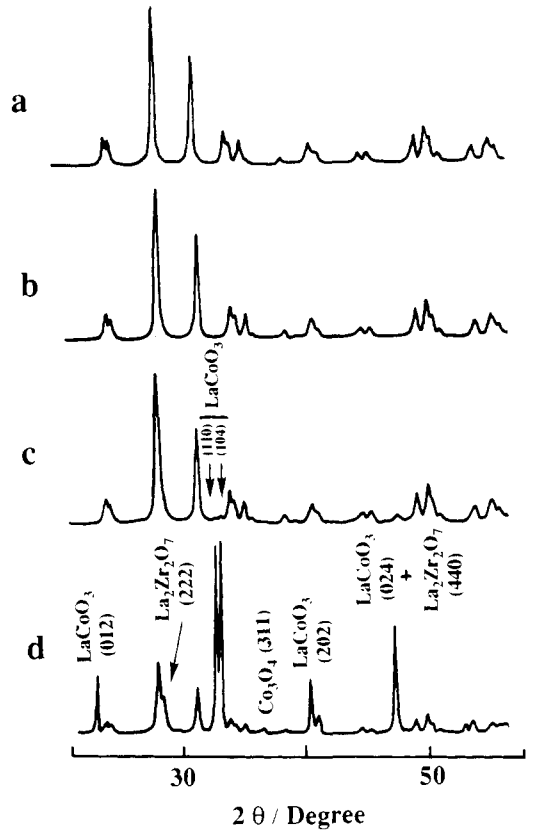

Figure 1. XRD patterns for La–Co/ZrO_2 calcined at 1123 K for 5 h: (a) ZrO_2; (b) La–Co(5.1 wt %)/ZrO_2; (c) La–Co(7.5 wt %)/ZrO_2; (d) La–Co(50 wt %)/ZrO_2.

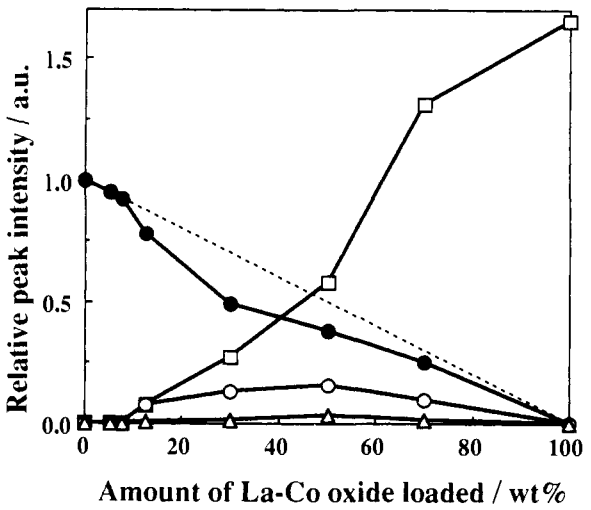

Figure 2. Changes in XRD main peak intensities of ZrO_2, $La_2Zr_2O_7$, Co_3O_4, and perovskite ($LaCoO_3$) phases with the amount of La–Co oxide loaded. The samples were calcined at 1123 K for 5 h: (●) ZrO_2; (○) $La_2Zr_2O_7$; (△) Co_3O_4; (□) perovskite ($LaCoO_3$). The main peak intensity of neat ZrO_2 was taken as unity. The calcination temperature was 1123 K. The broken line indicates the main peak intensity of ZrO_2 assuming that the intensity is proportional to the amount of ZrO_2 in La–Co/ZrO_2.

Figure 2 shows how the XRD intensities of the main peaks of each phase changed with the amounts of La–Co oxide loaded (calcined at 1123 K). The peak intensities of $La_2Zr_2O_7$ and Co_3O_4 appeared at the loading amount of 7.5 wt %, increased with the loading level up to 50 wt %, and then decreased. On the other hand, the intensities of ZrO_2 and $LaCoO_3$ monotonously decreased and increased, respectively, above 5 wt %.

The formation of $La_2Zr_2O_7$ and Co_3O_4 became clearer as the calcination temperature was increased. When the La–Co(5.1 wt %)/ZrO_2 was calcined at 1173 K, weak peaks appeared at 28.7° (shoulder, attributed to $La_2Zr_2O_7$), 32.9° ($LaCoO_3$), 33.3° ($LaCoO_3$), and 36.8° (Co_3O_4). The peak intensities of $La_2Zr_2O_7$ increased further by the calcination temperature at 1373 K. Figure 3 shows the effect of the calcination temperature for La–Co(30 wt %)/ZrO_2, for which the formation of $La_2Zr_2O_7$ and Co_3O_4 was distinct in Figure 1d. The XRD patterns were measured for the same sample after it was calcined for 1 h at each temperature, where the temperature was elevated stepwise in the range 773–1273 K. The peak intensity of $LaCoO_3$ increased with the calcination temperature up to 1073 K and then decreased in parallel with the peak intensity of ZrO_2. The peak intensities of Co_3O_4 and $La_2Zr_2O_7$ increased significantly above 1073 K.

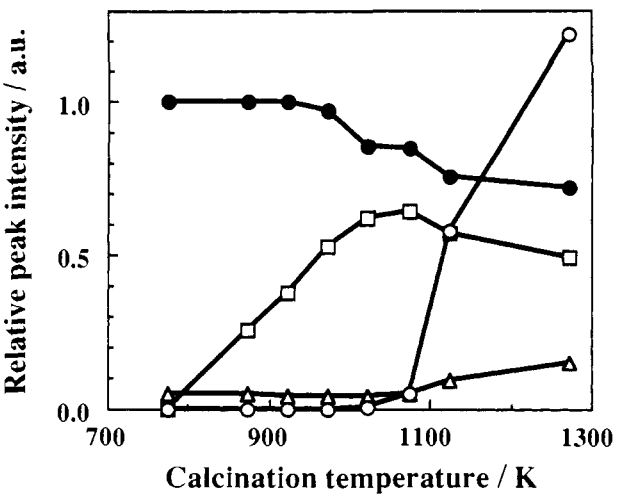

Figure 3. Plot showing the effects of calcination temperature on the formation of $La_2Zr_2O_7$, Co_3O_4, and perovskite phases. The symbols are the same as those in Figure 1. The main peak intensity was used as a measure of the formation of each phase. The main peak intensity of the ZrO_2 phase of La–Co oxide/ZrO_2 calcined at 773 K was taken as unity. The amount of La–Co oxide loaded was 30 wt %.

Table I. Formation of $LaCoO_3$, $La_2Zr_2O_7$, and Co_3O_4 Phases by Calcination at 1123 K[a]

sample no.	sample	phase observed		
		$LaCoO_3$	$La_2Zr_2O_7$	Co_3O_4
1	La/ZrO_2 (imp[b])	×[c]	×	×
2	La_2O_3 + ZrO_2 (mech[d])	×	×	×
3	$LaCoO_3$ + ZrO_2 (mech)	○[e]	○	○
4	La_2O_3 + Co_3O_4 + ZrO_2 (mech)	○	○	○
5	La–Co/ZrO_2 (imp[f])	○	○	○

[a] The amounts of La^{3+} and Co^{3+} in the samples were set to correspond to those of La^{3+} and Co^{3+} in La–Co(30 wt %)/ZrO_2, respectively. [b] ZrO_2 was impregnated with an aqueous solution of $La(OAc)_3$ by an incipient wetness method. [c] × indicates that no phases other than monoclinic ZrO_2 were detected. [d] The two or three oxides were mechanically mixed. [e] ○ indicates that the formation of $LaCoO_3$, $La_2Zr_2O_7$, or Co_3O_4 was detected. [f] ZrO_2 was impregnated with an aqueous solution of a stoichiometric mixture of cobalt and lanthanum acetates with respect to $LaCoO_3$ by an incipient wetness method.

Table I shows the formation of $La_2Zr_2O_7$, Co_3O_4, and $LaCoO_3$ phases for five samples. These samples had the same compositions, but they were prepared by mixing differently the La and Co compounds with ZrO_2. When ZrO_2 was impregnated with an aqueous solution of $La(OAc)_3$ (sample 1) or was mechanically mixed with La_2O_3 (sample 2), the $La_2Zr_2O_7$ formation was not observed after the samples were calcined at 1123 K. The formations of $La_2Zr_2O_7$ and Co_3O_4 were observed only when $LaCoO_3$ coexisted from the beginning or when $LaCoO_3$ was formed during the calcination (samples 3–5).

The formation of $LaCoO_3$ perovskite for La–Co(5.1–12.6 wt %)/ZrO_2 could not be confirmed by IR spectroscopy because of the overlapping of the intense IR bands of monoclinic ZrO_2 (750, 580, 500, 420 cm^{-1}) and $LaCoO_3$ perovskite (595, 565 (shoulder), 425 cm^{-1}). The IR spectra of monoclinic ZrO_2 and $LaCoO_3$ perovskite were approximately the same as those reported by

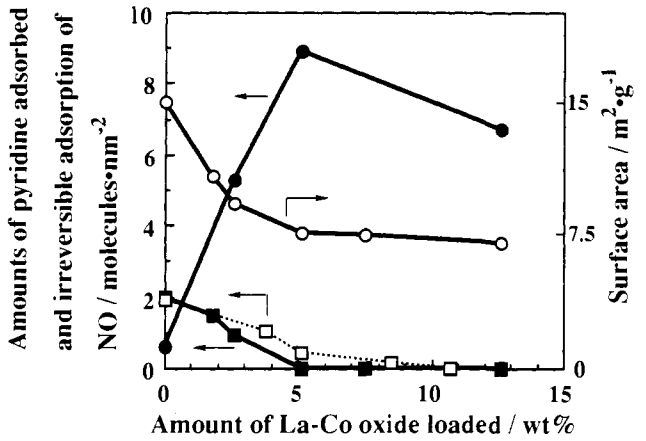

Figure 4. Plot showing the changes in the amount of NO adsorbed, surface area, and amount of pyridine adsorbed with the amount of La–Co oxide loaded: (●) amount of NO adsorbed; (○) specific surface area of La–Co/ZrO_2; (■) amount of pyridine adsorbed (ZrO_2, 15 $m^2 \cdot g^{-1}$); (□) amount of pyridine adsorbed (ZrO_2, 26 $m^2 \cdot g^{-1}$). The amount of pyridine adsorbed was estimated by the integrated IR peak intensity of pyridine (1446 cm^{-1}).

Table II. XPS Binding Energies (eV) for La–Co/ZrO_2[a]

amount of La–Co oxide loaded/wt %	Co $2p_{1/2}$ BE	Co $2p_{1/2}$ ΔS	Co $2p_{3/2}$ BE	Co $2p_{3/2}$ ΔS	ΔE	Zr $3d_{5/2}$	O 1s
0						182.4	530.3
1.8	796.3	n.d[b]	781.1	n.d[b]	15.2	182.2	530.1
2.6	796.1	8.2	780.9	6.4	15.2	182.2	530.4
5.1	796.1	7.9	780.8	6.4	15.3	182.2	530.3
7.5	796.1	8.5	780.7	6.7	15.4	182.0	530.0
$LaCoO_3$	796.2	7.8	780.8	7.4	15.3		529.0 531.7

[a] BE is the binding energy of the main signal; ΔS is the energy separation between the main signal and the satellite signal; ΔE is the spin-orbit splitting of the Co 2p level. Error limits are ±0.3 eV. [b] The satellite signal was too broad for the splitting to be determined.

McDevitt et al.[28] and Singh et al.[29] Neither the bands at 660 and 570 cm^{-1} characteristic of Co_3O_4[30] nor the bands at 610, 518, and 412 cm^{-1} of $La_2Zr_2O_7$[31] was detected for La–Co(5.1–12.6 wt %)/ZrO_2 samples. Such bands of $LaCoO_3$, Co_3O_4, and $La_2Zr_2O_7$ were observed for La–Co(30 wt %)/ZrO_2 calcined at 1273 K.

Adsorption of Pyridine and Nitrogen Monoxide. The IR spectra of pyridine adsorbed on ZrO_2 and La–Co/ZrO_2 showed the bands at 1608 (strong), 1574 (weak), 1488 (weak), and 1446 (strong) cm^{-1} in the range 1700–1400 cm^{-1} that are assignable to pyridine coordinated with Zr^{4+}, and no band due to protonated pyridine (e.g., 1535 cm^{-1}) was observed. The amounts of pyridine adsorbed on ZrO_2 having different surface areas of 15 and 26 $m^2 \cdot g^{-1}$ were estimated to be 2.0 and 1.9 molecules·nm^{-2}, respectively, using the absorption coefficient (0.146 $cm^2 \cdot \mu mol^{-1}$) of the 1446-cm^{-1} band.[32]

Figure 4 shows quantitatively the changes in the amounts of pyridine adsorbed (estimated by the intensity of the 1446-cm^{-1} band) with the amount of La–Co oxide loaded. The amount of pyridine adsorbed decreased with the amount of La–Co oxide loaded, and was almost zero at 5.1 wt %. The band at 1608 cm^{-1} varied in the same manner. The surface area also decreased, but to a much smaller extent than the decrease in the intensities of the 1446-cm^{-1} band. Hence, the trend was essentially the same when the intensities are normalized to the weight of catalysts.

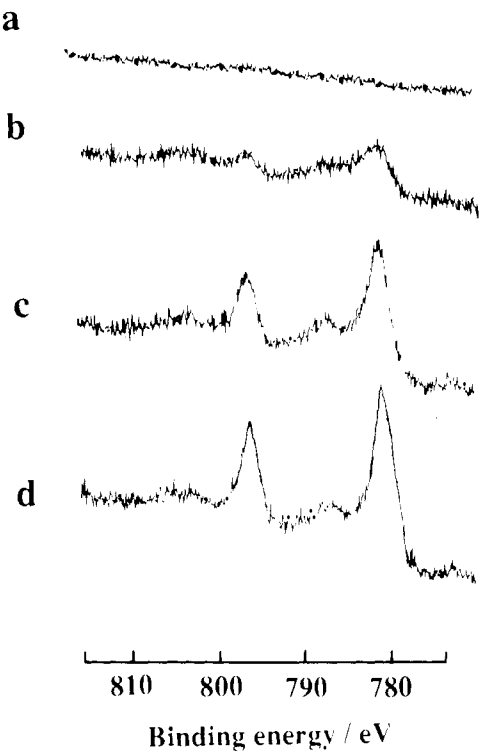

Figure 5. Co 2p photoelectron spectra for La–Co/ZrO_2: (a) ZrO_2; (b) La–Co(1.8 wt %)/ZrO_2; (c) La–Co(2.6 wt %)/ZrO_2; (d) La–Co(5.1 wt %)/ZrO_2.

Table III. Atomic Ratio of Co/La in La–Co/ZrO_2[a]

amount of La–Co oxide loaded/wt %	Co/La/au	amount of La–Co oxide loaded/wt %	Co/La/au
0		12.6	1.10
1.8	1.10	30	1.00
2.6	1.08	50	0.94
5.1	1.09	70	1.07
7.5	1.06	$LaCoO_3$	0.75

[a] Estimated by XPS peak intensity using the integrated areas of the Co $2p_{3/2}$ and La $3d_{5/2}$ and the sum of the integrated areas of Zr $3d_{5/2}$ and Zr $3d_{3/2}$ photoelectron lines.

In contrast with the pyridine adsorption, the amount of NO adsorbed increased until the loading level of 5.1 wt % was reached and then it slightly decreased. The amounts of NO adsorbed on La–Co(5.1 wt %)/ZrO_2 and $LaCoO_3$ perovskite were 5.4 and 5.2 molecules·nm^{-2}, respectively. It has been reported that the NO molecule interacts with surface Co, La, and oxide ions on La-CoO_3.[33]

Surface and Bulk Composition of Catalyst Particle. Figure 5 shows the Co 2p photoelectron spectra of La–Co/ZrO_2. The spectra exhibited a multiple splitting of 15.2–15.4 eV for Co^{3+} ions (see Table II). In the case of $LaCoO_3$, slight formation of Co^{2+} by reduction was indicated by the appearance of two satellite peaks (6–8 eV upscale from the peak for Co^{3+}), which are characteristic of Co^{2+} in a high-spin state and have been attributed to the shake-up excitation.[34] A similar slight reduction in the XPS chamber during the outgassing treatment has been reported previously,[35-37] and may be due to the desorption of adsorbed or

(28) McDevitt, M. T.; Baun, W. L. *J. Am. Ceram. Soc.* **1964**, *47*, 622–624.
(29) Singh, K. K.; Ganguly, P. *Spectrochim. Acta* **1984**, *40A*, 539–545.
(30) Nyquist, R. A.; Kagel, R. O. In *Infrared Spectra of Inorganic Compounds*; Academic Press: New York and London, 1971; p 219.
(31) Vandenborre, M. T.; Husson, E. *J. Solid State Chem.* **1983**, *50*, 362–371.
(32) Mizuno, N.; Take, J.; Yoneda, Y. *46th Symposium on Catalysis*; Sendai, Sept 1980.
(33) Tascon, J. M. D.; Tejuca, L. G.; Rochester, C. H. *J. Catal.* **1985**, *95*, 558–566.
(34) Tan, B. J.; Klabunde, K. J.; Sherwood, P. M. A. *J. Am. Chem. Soc.* **1991**, *113*, 855–861.
(35) Ichimura, K.; Inoue, Y.; Yasumori, I. *Bull. Chem. Soc. Jpn.* **1980**, *53*, 3044–3049.
(36) Marcos, J. A.; Buitrago, R. H.; Lombardo, E. A. *J. Catal.* **1987**, *105*, 95–106.
(37) Tejuca, L. G.; Bell, A. T.; Fierro, J. L. G.; Pena, M. A. *Appl. Surf. Sci.* **1988**, *31*, 301–316.

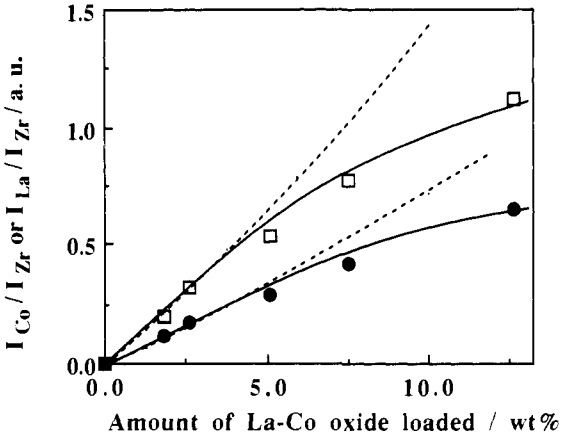

Figure 6. XPS intensity ratio ($I_{Co2p3/2}/I_{Zr(3d5/2+3d3/2)}$ and $I_{La3d5/2}/I_{Zr(3d5/2+3d3/2)}$) as a function of the amount of La–Co oxide was loaded: (●) $I_{Co2p3/2}/I_{Zr(3d5/2+3d3/2)}$; (□) $I_{La3d5/2}/I_{Zr(3d5/2+3d3/2)}$; broken line, calculated XPS intensity ratio of $I_{Co2p3/2}/I_{Zr(3d5/2+3d3/2)}$; dotted line, calculated XPS intensity ratio of $I_{La3d5/2}/I_{Zr(3d5/2+3d3/2)}$.

Table IV. Composition of La–Co/ZrO_2 Particles

amount of La–Co oxide loaded/wt %	composition of starting materials/%			composition of particles/%		
	La	Co	Zr	La	Co	Zr
0	0	0	100	0	0	100
2.6	1.3	1.3	97.4	1.8 ± 0.1	1.8 ± 0.1	96.4 ± 0.1
5.1	2.6	2.6	94.8	2.7 ± 0.2	2.4 ± 0.2	94.9 ± 0.4
7.5	3.8	3.8	92.4	4.0 ± 0.5	3.5 ± 0.5	92.5 ± 1.0
$LaCoO_3$	50	50	0	50 ± 3	50 ± 3	0

lattice oxygen, or the reaction with a small amount of contaminated reductants.

The binding energies of Co 2p, Zr $3d_{5/2}$, and O 1s peaks, energy separation between the main signal and satellite signal (ΔS), and spin–orbit splitting of the Co 2p level (ΔE) are given in Table II for La–Co/ZrO_2 samples and $LaCoO_3$. The observed values for Co were in general agreement with those of $LaCoO_3$ in Table II, as reported previously.[35-37] The positions of Zr $3d_{5/2}$ and O 1s lines changed little among the La–Co/ZrO_2 samples.

The O 1s spectrum of $LaCoO_3$ perovskite consisted of two peaks at around 532 and 529 eV, as in the literature.[34,36-39] The 532-eV peak has been assigned to hydroxide,[34] adsorbed water,[34] adsorbed oxygen,[37,38] and/or carbonate oxygen,[39] while the second peak is due to the lattice oxide ions.[34,36-39]

The relative intensities of the XPS line of Co or La to that of Zr are compared in Figure 6. The ratios $I_{Co2p3/2}/I_{Zr(3d5/2+3d3/2)}$ and $I_{La3d5/2}/I_{Zr(3d5/2+3d3/2)}$ (denoted by I_{Co}/I_{Zr} and I_{La}/I_{Zr}, respectively) increased linearly with the loading amount up to ca. 5 wt % and deviated to a lower side at higher loadings.

The surface compositions of the metallic components are calculated from the integrated intensity of the XPS lines with eq 1 as summarized in Table III. The La content was close to that of Co in each of the La–Co/ZrO_2 samples, while the content of La was a little greater than that of Co in the neat $LaCoO_3$ perovskite as reported previously.[40]

Table IV summarizes the compositions of five samples that were measured particle by particle by EDX. For each loading amount of La–Co oxide, the composition was very close to that calculated by the composition of starting materials used for the impregnation. The observed Co/La ratio in $LaCoO_3$ perovskite was about unity in agreement with the Co/La ratio (0.99) determined by atomic absorption spectroscopy.[41] TEM and EDX observation did not detect any segregated particles of perovskite in La–Co(0–7.5 wt %)/ZrO_2, but they did detect segregated $LaCoO_3$ perovskite particles in La–Co(≥30 wt %)/ZrO_2.

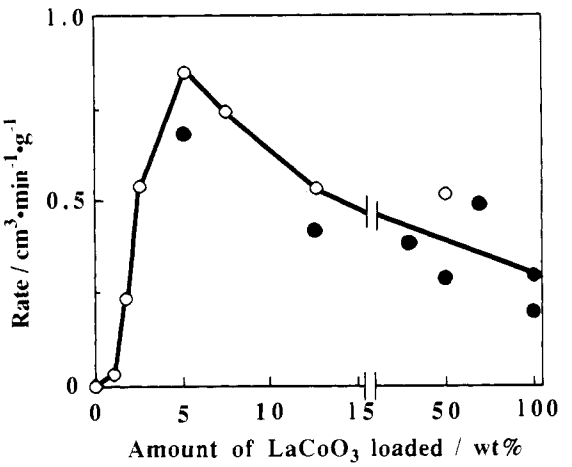

Figure 7. Effects of the amount of La–Co oxide loaded on the catalytic activity for the oxidation of propane: (○) impregnation was repeated several times; (●) impregnation was carried out in a single step; reaction temperature, 548 K.

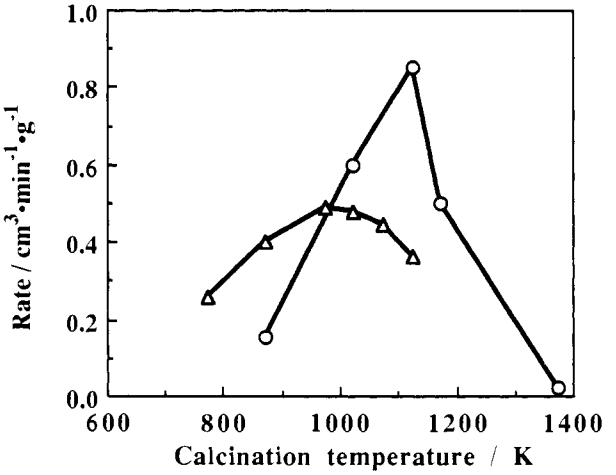

Figure 8. Effect of the calcination temperature of La–Co/ZrO_2 on the catalytic activity for the oxidation of propane at 548 K: (○) La–Co(5.1 wt %)/ZrO_2; (△) La–Co(30 wt %)/ZrO_2.

Table V. Rate of Oxidation of Propane at 548 K

catalyst[a]	rate/$cm^3 \cdot min^{-1} \cdot g^{-1}$
La–Co (5.1 wt %)/ZrO_2	0.85 (0.11)[b]
Co_3O_4 (1.7 wt %)/ZrO_2[c]	0.11 (0.03)
$LaCoO_3$	0.20 (0.14)

[a] Calcination temperature, 1123 K. [b] Numbers in parentheses are the rates per specific surface area ($cm^3 \cdot min^{-1} \cdot m^{-2}$). [c] ZrO_2 was impregnated with an aqueous solution of $Co(CH_3COO)_2$ by an incipient wetness method.

Catalytic Activity for Oxidation. The catalytic activities for the complete oxidation of propane over La–Co/ZrO_2 are shown in Figure 7. The rate increased linearly at first with the increase in the amount of La–Co oxide loaded and then gradually decreased showing a maximum at 5.1 wt %.

Figure 8 shows the effect of the calcination temperature for La–Co(5.1 and 30 wt %)/ZrO_2 on the catalytic activity at 548 K. La–Co(5.1 and 30 wt %)/ZrO_2 samples of which the XRD data are shown in Figure 3 were used for the activity measurements.

The catalytic activity of La–Co(5.1 wt %)/ZrO_2 for the oxidation of propane at 548 K was compared with that of the $LaCoO_3$

(38) Pena, M. A.; Tascon, J. M. D.; Fierro, J. L. G.; Tejuca, L. G. *J. Colloid Interface Sci.* **1987**, *119*, 100–107.
(39) Lombardo, E. A.; Tanaka, K.; Toyoshima, I. *J. Catal.* **1983**, *80*, 340–349.
(40) Nitadori, T.; Ichiki, T.; Misono, M. *Bull. Chem. Soc. Jpn.* **1988**, *61*, 621–626.
(41) Mizuno, N.; Tanaka, M.; Misono, M. *J. Chem. Soc., Faraday Trans I* **1992**, *88*, 91–95.

Table VI. Parameters Used in the Calculation of I_{Co}/I_{Zr}

IMFP of the Co $2p_{3/2}$ photoelectron in $LaCoO_3$ perovskite	$\lambda_{Pero,Co}$	0.763 nm
IMFP of the La $3d_{5/2}$ photoelectron in $LaCoO_3$ perovskite	$\lambda_{Pero,La}$	0.700 nm
IMFP of the Zr $3d_{5/2}$ photoelectron in $LaCoO_3$ perovskite	$\lambda_{Pero,Zr}$	1.42 nm
IMFP of the Zr $3d_{5/2}$ photoelectron in ZrO_2	$\lambda_{Zr,Zr}$	1.48 nm
no. of Zr atoms in the unit volume of ZrO_2	d_{Zr}	28.8 nm^{-3}
no. of Co atoms in the unit volume of $LaCoO_3$	d_{Co}	17.9 nm^{-3}
thickness of the ideal $LaCoO_3$(100) monolayer	t	0.382 nm
weight of the ideal $LaCoO_3$(100) monolayer	A	2.80×10^{-3} $g \cdot m^{-2}$

perovskite in Table V. The activity per weight of La–Co(5.1 wt %)/ZrO_2 was greater than that of Co_3O_4(1.7 wt %)/ZrO_2 and $LaCoO_3$ perovskite, and comparative to that of $La_{0.8}Sr_{0.2}CoO_3$ perovskite. The activity per specific surface area of La–Co(5.1 wt %)/ZrO_2 was comparable to that of $LaCoO_3$ perovskite (see numbers in parentheses in Table V). The catalytic activities of ZrO_2, La_2O_3, and $La_2Zr_2O_7$ for the oxidation were much lower than that of Co_3O_4(1.7 wt %)/ZrO_2.

Discussion

Dispersion of La–Co Oxide (≤5.1 wt %) on ZrO_2. The IR spectra of pyridine adsorbed on ZrO_2 and on La–Co/ZrO_2 showed the bands characteristic of pyridine coordinated with Zr^{4+} (Lewis acid site) as reported previously.[32] As shown by solid squares in Figure 4, these IR bands decreased with the loading of La–Co oxide and almost disappeared at 5.1 wt %. This result shows that as the loading level of La–Co oxide was increased the surface of ZrO_2 was covered to an extent approximately proportional to the loading amount and fully covered at about 5 wt % loading by a substance inactive to pyridine chemisorption.

By contrast, the amount of NO irreversively adsorbed was small on ZrO_2 and increased linearly with the loading level up to 5 wt % (solid circles in Figure 4). Therefore, the substance covered the surface in proportion to the loading amount and is not active for pyridine chemisorption but active for NO chemisorption. XRD detected no phases other than monoclinic ZrO_2 for these samples, and TEM and EDX did not detect any segregated particles of perovskite up to the loading level of 7.5 wt %. These results indicate that the supported substance was highly dispersed as fine particles or thin overlayers on the surface of ZrO_2 up to 5.1 wt %. In accordance with this idea, the loading level of 5 wt % corresponds to the order of monolayer to bilayer coverage of $LaCoO_3$ perovskite on ZrO_2.[42]

The changes in the XPS peak intensities with the loading amount are consistent with the high dispersion of $LaCoO_3$ perovskite, as in the case of V_2O_5/SiO_2.[43] The overlayer is assumed to have a (100) layer of $LaCoO_3$ perovskite, the coverage and the thickness being θ and t, respectively. The parameters used in this calculation are given in Table VI. The values of d_{Co} or t and d_{Zr} are derived from the crystallographic data of $LaCoO_3$ perovskite[44] and ZrO_2,[45] respectively, and $\lambda_{Pero,Co}$, $\lambda_{Pero,La}$, $\lambda_{Zr,Zr}$, and $\lambda_{Pero,Zr}$ are calculated according to the literature.[46] Then the XPS intensity ratio, I_{Co}/I_{Zr}, is expressed by

$$\frac{I_{Co}}{I_{Zr}} = \frac{\sigma_{Co}\lambda_{Pero,Co}d_{Co}\theta(1 - \exp(-Nt/\lambda_{Pero,Co}))}{\sigma_{Zr}\lambda_{Zr,Zr}d_{Zr}(1 - \theta + \theta\exp(-Nt/\lambda_{Pero,Zr}))} \quad (2)$$

where σ_{Co} and σ_{Zr} are the ionization cross sections for Co and Zr, respectively.[26] θ can be expressed by the equation

$$\theta = w/(SAN) \quad (3)$$

where w, A, S are the weight ratio of $LaCoO_3$ loaded and ZrO_2, the weight of an ideal $LaCoO_3$ perovskite (100) monolayer of unit area, and the specific surface area of the support (15 $m^2 \cdot g^{-1}$), respectively.

The calculated I_{Co}/I_{Zr} and I_{La}/I_{Zr} are also given by the dotted and broken lines in Figure 6, respectively, for $N = 1$. When $N = 2$, I_{Co}/I_{Zr} calculated decreases by ca. 20% below the loading level of 5 wt %. When N varies from 2 to 10, I_{Co}/I_{Zr} and I_{La}/I_{Zr} increase by a factor of about 3. Since the loading amount of 5 wt % approximately corresponds to that of monolayer or bilayer on the surface of ZrO_2 (15 $m^2 \cdot g^{-1}$),[42] the small values of N (1 or 2) supports the high dispersion of La–Co oxide on ZrO_2. Deviation at higher loading levels (≥5.1 wt %) can be explained by the reaction between $LaCoO_3$ formed and ZrO_2 (see later section).

Structure of La–Co Oxide (≤5.1 wt %) on ZrO_2. The composition of each particle measured by EDX for La–Co(≤7.5 wt %)/ZrO_2 (Table IV) and the XPS data in Table III show that each ZrO_2 particle was uniformly impregnated by the substance having the Co/La ratio of 1.0. The XPS data in Table II are in general agreement with those of $LaCoO_3$ perovskite, and the $LaCoO_3$ perovskite structure became detectable by XRD when the loading level slightly exceeded 5.1 wt %. In addition, the amount of NO adsorbed on La–Co(5.1 wt %)/ZrO_2 (5.4 molecules·nm^{-2}) agreed well with that adsorbed on $LaCoO_3$ perovskite (5.2 molecules·nm^{-2}). The amount of NO adsorbed was a little smaller than that reported in ref 33, probably due to the lower equilibrium pressure of NO in this work. Hence, it may be concluded that "$LaCoO_3$ perovskite or the like" was formed in highly dispersed states on the surface of ZrO_2 below the loading level of about 5 wt %. The fact that the activity per specific surface area of La–Co(5.1 wt %)/ZrO_2 was comparable to that of $LaCoO_3$ perovskite (Table V) is consistent with the formation of highly dispersed $LaCoO_3$ perovskite on the surface of ZrO_2.

The formation of $LaCoO_3$ seems possible, since the structure of the $LaCoO_3$ perovskite fits geometrically the surface of ZrO_2 as discussed below. It has been reported that the (100) plane (by the expression of the cubic structure of $LaCoO_3$[44]) containing transition metals is likely an active reaction surface in electrocatalysis and heterogeneous catalysis.[35,47] The (001) plane is the cleavage plane of monoclinic ZrO_2.[45] Although geometrical fitting is not found between the (100) plane of $LaCoO_3$[44] and either the (001), (111), (110) plane of monoclinic ZrO_2,[45] good fitting exists between the (100) plane of $LaCoO_3$ perovskite and the (001) plane of tetragonal[48] or cubic[49] ZrO_2 as shown in Figure 9, where oxide ion is located at each apex of the dashed squares and the distance between neighboring oxide ions is in the range of 2.6–2.7 Å. It is probable that the surface oxide ion of monoclinic ZrO_2 with only slight displacement rearranges to that of tetragonal or cubic ZrO_2 during the formation of $LaCoO_3$ perovskite on ZrO_2. A similar fitting is also observed between the (200) plane of $LaCoO_3$ perovskite and the (001) plane of cubic ZrO_2.

The bonding between cubic ZrO_2 and $LaCoO_3$ may be further speculated as below. When the dashed square of Figure 9c is superposed on that of Figure 9b, the Zr atoms of the (001) plane of cubic ZrO_2 are bound to O atoms of the (001) plane of $LaCoO_3$ with the coordination number of 8, the same as that in the ZrO_2 bulk, and the bond angles and the bond lengths remain almost unchanged. On the other hand, the greater changes in the coordination numbers are necessary when the (200) plane of $LaCoO_3$ is placed on the (001) plane of cubic ZrO_2. Hence, the former is the more probable structure.

Solid-State Reaction of La–Co Oxide with ZrO_2. The relative XRD line intensity of ZrO_2 is calculated by assuming that the intensity is proportional to the content of ZrO_2 in La–Co/ZrO_2, as shown by the broken line in Figure 2. The observed intensity

(42) Monolayer of (100) layer of $LaCoO_3$ perovskite containing Co^{3+} and O^{2-}ions on the surface of ZrO_2 having the surface area of 15 $m^2 \cdot g^{-1}$ corresponds to 4 wt % loading of La–Co oxide. If one assumes, for example, bilayers of (100) plane, the coverage at this loading level becomes 0.5.

(43) Inumaru, K.; Okuhara, T.; Misono, M. *J. Phys. Chem.* **1991**, *95*, 4826–4832.
(44) Wold, A.; Post, B.; Banks, E. *J. Am. Chem. Soc.* **1957**, *79*, 6365–6366.
(45) Smith, D. K.; Newkirk, H. W. *Acta Crystallogr.* **1965**, *18*, 983–991.
(46) Penn, D. R. *J. Electron Spectrosc. Relat. Phenom.* **1976**, *9*, 29–40.
(47) Bokris, J. O'M.; Otagawa, T. *J. Electrochem. Soc.* **1984**, *131*, 290–302.
(48) Wolten, G. M. *Acta Crystallogr.* **1964**, *17*, 763–765.
(49) Smith, D. K.; Cline, C. F. *J. Am. Ceram. Soc.* **1962**, *45*, 249–250.

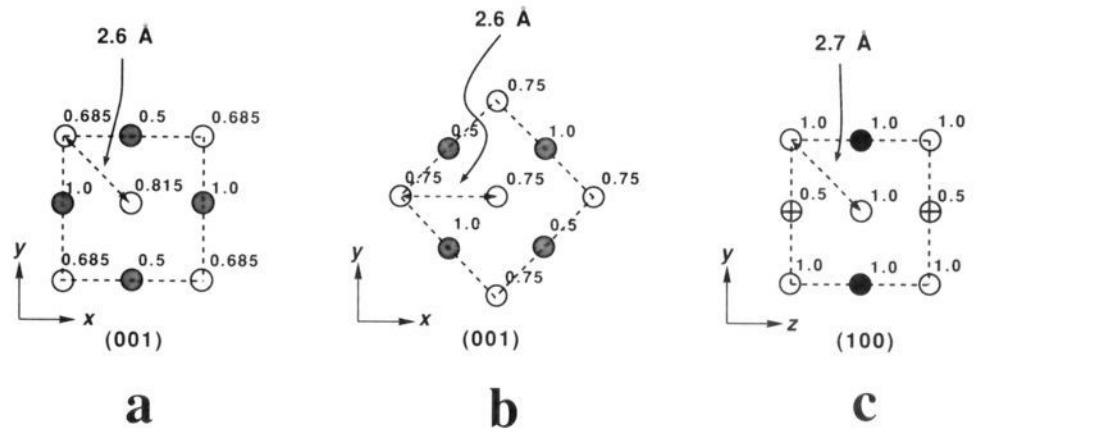

Figure 9. Projection of structures of tetragonal and cubic ZrO_2 parallel to the z direction onto the x–y plane and $LaCoO_3$ parallel to the x direction on the y–z plane: (a) tetragonal ZrO_2, (b) cubic ZrO_2, (c) $LaCoO_3$ (by the expression of the cubic structure); (◎) Zr, (●) Co, (⊕) La, (○) O. The numbers represent the z and x coordinates for each atom in terms of c and a, respectively.

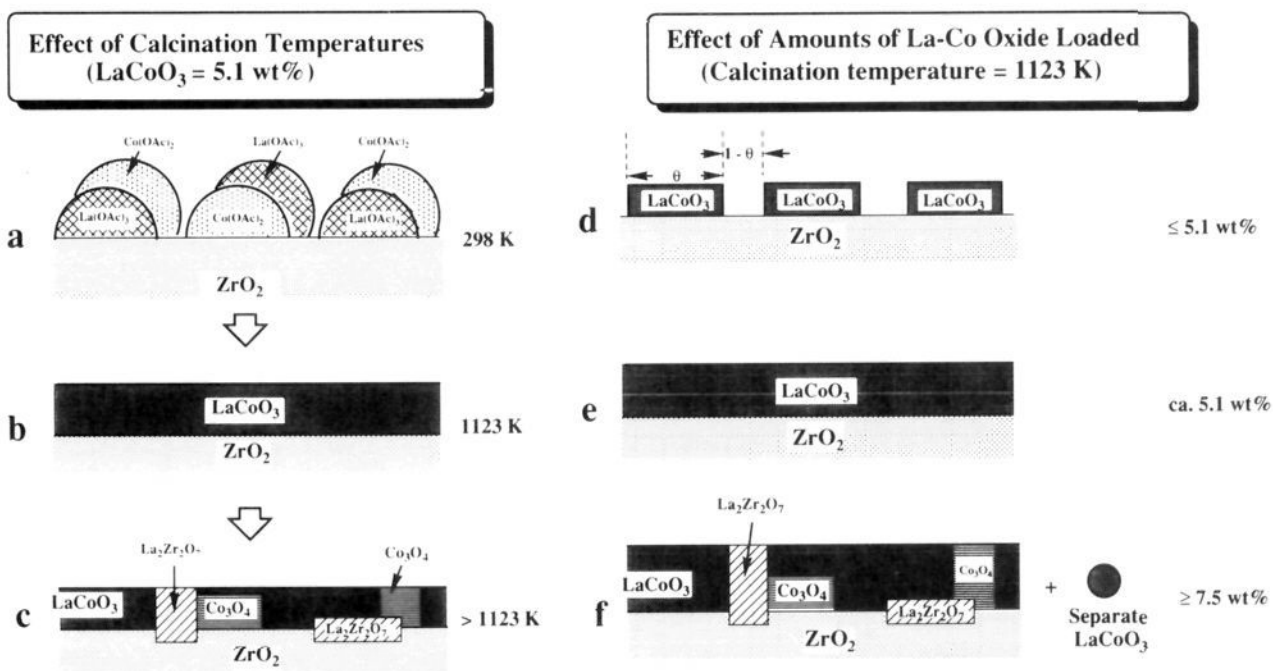

Figure 10. Proposed model of La–Co/ZrO_2. The numbers are the amount of La–Co oxide loaded and the calcination temperatures, θ and t, see Discussion.

of ZrO_2 (solid circles) agreed with the calculated value up to the loading level of 5.1 wt %, indicating that no reaction occurs between ZrO_2 support and substance supported up to this loading level. On the other hand, above 5.1 wt %, the line intensity of ZrO_2 deviated to the lower side of the broken line and the XRD intensity of the Co_3O_4 phase changed in parallel with that of the $La_2Zr_2O_7$ phase as shown in Figures 1 and 2, showing that Co_3O_4 and $La_2Zr_2O_7$ were formed by the concurrent or the same reaction(s).

The peak intensities of above two phases monotonously increased at first, but decreased above 50 wt % as shown in Figure 2. TEM and EDX detected segregated $LaCoO_3$ perovskite particles for La–Co(≥30 wt %)/ZrO_2. Therefore, separate $LaCoO_3$ perovskite particles were probably formed above 7.5 wt %. The formation of separate $LaCoO_3$ particles depended on the amount of La–Co oxide loaded and the calcination temperature of La–Co/ZrO_2.

The catalytic activity for oxidation is in the order of La–Co/ZrO_2 > Co_3O_4/ZrO_2 ≫ ZrO_2, $La_2Zr_2O_7$ (see Results and Table V). (The Co content in 5.1 wt % $LaCoO_3$ is equal to that in 1.7 wt % Co_3O_4.) Therefore, the lower activity of La–Co(5.1 wt %)/ZrO_2 calcined at 1373 K than that calcined at 1123 K as shown in Figure 8 is explained by the greater extent of progress of the formation of $La_2Zr_2O_7$ and Co_3O_4 on the surface of La–Co/ZrO_2 at the higher calcination temperature. The decrease in the amount of NO adsorbed on La–Co/ZrO_2 above the loading level of 5.1 wt % is also consistent with the formation of $La_2Zr_2O_7$ and/or Co_3O_4 on the surface if one considers the report that the amount of NO adsorption on $LaCoO_3$ was greater than that on Co_3O_4.[33,50]

Proposed Model for Formation of La–Co Oxide on ZrO_2. The model of the formation of La–Co oxide on ZrO_2 is shown in Figure 10 based on the discussion as described above. Here, the amount and size of each phase or particle formed is not explicitly considered. In the adsorption experiments in aqueous solution, the amounts of La and Co ions contained in the filtrate reached a constant after 1 h and the amounts of La and Co ions adsorbed on ZrO_2 were 1.6 and 0.72 molecules·nm^{-2}, respectively, i.e., the amount of Co ion adsorbed on ZrO_2 corresponded to about half the amount of La ion. On the basis of these results, the state of the surface of ZrO_2 just after impregnation is speculated as shown in Figure 10a.

(50) Yao, H. C.; Shelef, M. *J. Phys. Chem.* **1974**, *78*, 2490–2496.

When La-Co/ZrO_2 was calcined at 1123 K, $LaCoO_3$ perovskite or the like is formed in a highly dispersed state as fine particles or thin overlayers on the surface of ZrO_2 below the loading level of about 5 wt % (Figure 10, b and e).

The reaction between the substance (La-Co oxide) and ZrO_2 to form $La_2Zr_2O_7$ and Co_3O_4 occurred by the calcination above 1123 K and at and above the loading amount of 7.5 wt % (Figure 10, c and f). In these models, $La_2Zr_2O_7$ is formed in contact with ZrO_2 because the structure of pyrochlore $La_2Zr_2O_7$ is very close to that of tetragonal or cubic ZrO_2. The formation of $La_2Zr_2O_7$, Co_3O_4, and $LaCoO_3$ was observed in the XRD pattern of La-Co(5.1 wt %)/ZrO_2 calcined at 1373 K and the IR spectrum of La-Co(30 wt %)/ZrO_2 calcined at 1273 K, suggesting the model shown in Figure 10c.

Acknowledgment. The authors acknowledge JEOL for the EDX measurements. This work was supported in part by a Grant-in-Aid from the Ministry of Education, Science and Culture of Japan.

Registry No. La, 7439-91-0; Co, 7440-48-4; ZrO_2, 1314-23-4; NO, 10102-43-9; pyridine, 110-86-1.

Infrared Multiple Photon Dissociation of Acetone Radical Cation. An Enormous Isotope Effect with No Apparent Tunneling

Thomas H. Osterheld and John I. Brauman*

Contribution from the Department of Chemistry, Stanford University, Stanford, California 94305-5080. *Received February 18, 1992*

Abstract: Infrared multiple photon dissociation experiments on acetone cation and d_6-acetone cation indicate that the hydrogen atom abstraction resulting in methane loss does not involve tunneling. The large isotope effect arises from a competitive mechanism. Reaction thresholds and zero point vibrational energy differences indicate that the critical energy for methane loss is up to 0.9 kcal/mol below the threshold for loss of methyl radical in the unlabeled acetone cation system.

Reactions that may involve tunneling through potential barriers are an exciting area of study.[1] Tunneling is difficult to investigate experimentally, as discussed recently by Baer and co-workers;[2] classical barriers in the potential-energy surface cannot be measured experimentally, so that tunneling must be inferred from other methods such as isotope effect measurements. However, care must be taken to also consider changes in zero point vibrational energies (ZPVE) which give rise to "classical" isotope effects.

Recently it was proposed that methane elimination from acetone radical cation proceeds by a tunneling mechanism.[3] This reaction involves a hydrogen atom transfer step, and the metastable ion[4] of 1,1,1-d_3-acetone cation yields an enormous 70/1 preference for methane loss by hydrogen atom abstraction as opposed to deuterium atom abstraction[5] (eq 1).

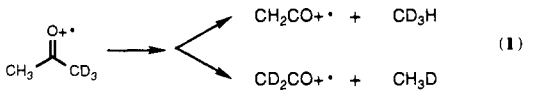

(1)

It would be surprising if this result arises from a "classical" isotope effect.[6] We show here, however, with infrared multiple photon (IRMP) dissociation[7-10] experiments on acetone cation and d_6-acetone cation, that methane loss does not occur by a tunneling mechanism.[11] The large apparent preference for abstraction of hydrogen arises from a phenomenon which we term a "competitive reaction isotope effect". Large isotope effects can be observed in metastable ions because they usually involve a narrow energy range near threshold. In this case, however, the large isotope effect arises from a competition between reactions and is not a consequence of the measurement technique or the range of energies populated by the experiment.

Systems that involve loose and tight transition states at similar energies may display competitive reaction isotope effects. In particular, we expect that this behavior will be encountered in other ion systems. Considerable evidence indicates that many low-energy reactions of gas-phase ions involve ion-neutral complexes.[12-19] Methane elimination from acetone cation belongs to a common class of reactions[15] (eq 2) which involve a bond cleavage to form an ion-neutral complex followed by a hydrogen atom abstraction by the neutral fragment. Inherent in this mechanism is the competition between a loose transition state (complete cleavage to separated products) and a tight transition state (hydrogen atom abstraction). Hydrogen atom abstraction can be observed if its

(1) Bell, R. P. *The Tunnel Effect in Chemistry*; Chapman and Hall Ltd.: New York, NY, 1980.
(2) Booze, J. A.; Weitzel, K.-M.; Baer, T. *J. Chem. Phys.* **1991**, *94*, 3649.
(3) Heinrich, N.; Louage, F.; Lifshitz, C.; Schwarz, H. *J. Am. Chem. Soc.* **1988**, *110*, 8183.
(4) Cooks, R. G.; Beynon, J. H.; Caprioli, R. M.; Lester, G. R. *Metastable Ions*; Elsevier Scientific Publishing Company: New York, NY, 1973.
(5) Lifshitz, C.; Tzidony, E. *Int. J. Mass. Spectrom. Ion Phys.* **1981**, *39*, 181.
(6) Recent experiments showing bond-specific reactivity display enormous isotope effects. (a) Bronikowski, M. J.; Simpson, W. R.; Girard, B.; Zare, R. N. *J. Chem. Phys.* **1991**, *95*, 8647. (b) Sinha, A.; Hsiao, M. C.; Crim, F. F. *J. Chem. Phys.* **1990**, *92*, 6334. (c) Sinha, A.; Hsiao, M. C.; Crim, F. F. *J. Chem. Phys.* **1991**, *94*, 4928.
(7) Lupo, D. W.; Quack, M. *Chem. Rev.* **1987**, *87*, 181.
(8) Quack, M. *J. Chem. Phys.* **1978**, *69*, 1282.
(9) Quack, M.; Seyfang, G. *J. Chem. Phys.* **1982**, *76*, 955.
(10) Dunbar, R. C. *J. Chem. Phys.* **1991**, *95*, 2537.
(11) Truhlar and co-workers have shown that many hydrogen atom transfer reactions involve aspects that can be attributed to tunneling. See: Garrett, B. C.; Truhlar, D. G.; Wagner, A. F.; Dunning, T. H., Jr. *J. Chem. Phys.* **1983**, *78*, 4400. Our experiments on acetone cation demonstrate that the barrier to hydrogen atom transfer lies below the endothermic threshold for methyl radical loss and that hydrogen atom transfer is not required to occur by tunneling *through* a potential barrier.
(12) Bowen, R. D. *Acc. Chem. Res.* **1991**, *24*, 364.
(13) Hammerum, S.; Audier, H. A. *J. Chem. Soc., Chem. Commun.* **1988**, 860.
(14) Lifshitz, C.; Rejwan, M.; Levin, I.; Peres, T. *Int. J. Mass. Spectrom. Ion Processes* **1988**, *84*, 271.
(15) McAdoo, D. J.; Hudson, C. E. *Int. J. Mass. Spectrom. Ion Processes* **1984**, *59*, 325.
(16) McAdoo, D. J. *Mass Spectrom. Rev.* **1988**, *7*, 363.
(17) Morton, T. H. *Tetrahedron* **1982**, *38*, 3195.
(18) Morton, T. H. *Org. Mass. Spectrom.* **1992**, *27*, 353.
(19) Longevialle, P.; Botter, R. *Org. Mass. Spectrom.* **1983**, *18*, 1.

0002-7863/92/1514-7158$03.00/0